Journal of Mechanical Design and Testing 8(1), (2026), 21-33
DOI: 10.22146/jmdt.121141
e-ISSN: 2685-8029, ISSN: 2716-1293

Electrochemical Performance of Modified Graphite Anode Materials for Lithium-Ion Batteries*

E. Prasetya[1]*, W.A. Pardede[1], A. Rifai[2], M.D. Raditya[1], Fawaidzdurahman[1] and Y. Hidayat[1]

[1]PLN Indonesia Power, Jakarta Indonesia
[2]BRIN-Pusat Riset Material Maju, Jakarta Indonesia
*E-mail: eko.prasetya@plnindonesiapower.co.id

Abstrak

Penelitian ini menyelidiki sintesis dan karakterisasi anoda grafit termodifikasi secara kimia pada skala pilot untuk baterai ion litium (*lithium-ion batteries*, LIB), dengan menggunakan etsa kalium hidroksida (KOH) untuk meningkatkan sifat permukaan dan kapasitas penyimpanan litium. Proses modifikasi yang berbiaya rendah dan mudah diskalakan ini menghasilkan peningkatan jarak antar lapisan (*interlayer spacing*), sebagaimana dikonfirmasi melalui analisis difraksi sinar-X (*X-ray diffraction*, XRD), yang menunjukkan terjadinya transformasi struktur secara berhasil. Analisis mikroskop elektron pemindai (*scanning electron microscopy*, SEM) mengungkapkan perubahan morfologi yang signifikan berupa peningkatan porositas, sementara analisis luas permukaan spesifik menggunakan metode *Brunauer–Emmett–Teller* (BET) menunjukkan peningkatan yang substansial dari 10 m^2/g menjadi 80 m^2/g, yang mengonfirmasi terbentuknya struktur berpori. Analisis termogravimetri dan spektroskopi inframerah transformasi Fourier (*Fourier-transform infrared spectroscopy*, FTIR) menunjukkan stabilitas termal yang tinggi serta tingkat fungsionalisasi permukaan yang minimal. Kinerja elektrokimia dievaluasi menggunakan sel silinder tipe 18650 dengan katoda $LiFePO_4$ (LFP). Sel pada Batch 4 dan Batch 5 menunjukkan rasio N/P yang optimal, yaitu 1,2–1,3, sehingga menghasilkan peningkatan kapasitas spesifik dan stabilitas siklus. Di antara seluruh batch yang diuji, Batch 6 menunjukkan retensi kapasitas dan efisiensi coulombik tertinggi selama pengujian performa pada berbagai laju pengosongan (*rate performance testing*). Hasil penelitian ini menunjukkan potensi grafit termodifikasi KOH sebagai material anoda berkinerja tinggi serta memberikan wawasan penting mengenai strategi produksi yang dapat diskalakan untuk pengembangan baterai ion litium generasi berikutnya.

***Kata kunci**: Anoda grafit, kalium hidroksida, baterai ion litium, sistem penyimpanan energi.*

Abstract

This study investigates the pilot-scale synthesis and characterization of chemically modified graphite anodes for lithium-ion batteries (LIBs), using potassium hydroxide (KOH) etching to enhance surface properties and lithium storage capacity. The low-cost, scalable modification process led to increased interlayer spacing, as confirmed by X-ray diffraction (XRD), indicating successful structural transformation. Scanning electron microscopy (SEM) analysis revealed significant morphological changes with increased porosity, while Brunauer–Emmett–Teller (BET) surface analysis showed a substantial rise in specific surface area, from 10 m^2/g to 80 m^2/g, confirming the formation of porous structures. Thermogravimetric and Fourier-transform infrared spectroscopy (FTIR) analyses demonstrated high thermal stability and minimal surface functionalization, respectively. Electrochemical performance was evaluated using 18650 cylindrical cells with $LiFePO_4$ (LFP) cathodes. Batch 4 and 5 cells exhibited optimal N/P ratios of 1.2–1.3, achieving improved specific capacity and cycle stability. Among all batches, Batch 6 demonstrated the highest capacity retention and coulombic efficiency during rate performance testing. These results highlight the potential of KOH-modified graphite as a high-performance anode material and offer valuable insights into scalable production strategies for next-generation LIBs.

***Keywords**: Graphite anode, potassium hydroxide, lithium-ion batteries, energy storage systems.*

Best paper dalam SCIENCE TECHNOLOGY AND MANAGEMENT MEETUP (STeM MEET UP) 2025, PT. PLN Indonesia Power, 26 November 2025 di Gumaya Tower Hotel Semarang.

1. INTRODUCTION

Energy storage technologies have become increasingly essential as the global energy landscape shifts towards renewable energy sources and electric mobility (Amir *et al*, 2023). Lithium-ion batteries are one of the most advanced alternative energy storage devices today owing to their high energy density, long cycle life, and environmental compatibility (Wang *et al*, 2019)(Ngoy *et al*, 2025). Their widespread application spans from portable electronics to electric vehicles and grid-scale storage, driving continuous innovation in battery materials and architectures (Sergi *et al*, 2016). However, meeting the growing performance demands, such as faster charging, longer lifespan, and higher capacity, requires breakthroughs in electrode design and material engineering. In particular, optimizing anode materials has become a focal point for enhancing overall battery efficiency and reliability.

The use of graphite as anode in LIBs has become dominant in industry for the past few decades due to its ability to offer a balance between storage energy capacity and long cycle life. Its layered structure enables reversible lithium-ion intercalation, offering a theoretical capacity of 372 mAh/g and a low operating potential (~0.1 V vs. Li/Li^+) (Yang *et al*, 2024)(Yao *et al*, 2023). However, as the performance demands of LIBs intensify, particularly for fast-charging and high-capacity applications, pristine graphite faces limitations in rate capability, surface reactivity, and lithium-ion diffusion kinetics (Chen *et al*, 2025). To overcome these challenges, various strategies have been explored to modify graphite and enhance its electrochemical performance, including surface coating (Oka *et al*, 2022), heteroatom doping (Bao *et al*, 2023), hybridization (He *et al*, 2021), and chemical modification (Kim *et al*, 2020).

Among these approaches, chemistry modification of graphite surface with activating agents such as potassium hydroxide (KOH) has gained significant attention due to its simplicity, scalability, and cost-effectiveness (Schultz *et al*, 2000). The KOH activation process is known to produce micropores on the graphite surface, which increases the specific surface area and expands the interlayer spacing of graphite, thereby enhancing lithium-ion accessibility and storage capacity (Kim *et al*, 2020). The process also introduces edge defects and oxygen-containing functional groups, which can improve wettability and electrochemical activity without compromising structural integrity (Kim *et al*, 2020). Compared to other activation methods, such as plasma treatment or metal oxide deposition, KOH etching offers a more sustainable and industrially viable route for large-scale production of modified graphite anodes (Howe *et al*, 2003).

In this study, we present a pilot-scale synthesis and comprehensive characterization of KOH-etched graphite anodes, focusing on their structural evolution, surface properties, and electrochemical performance in 18650 cylindrical cells. The findings aim to bridge the gap between laboratory-scale innovations and practical implementation in next-generation lithium-ion batteries.

2. METHODS

Modified graphite anodes were synthesized via alkaline etching using synthetic graphite powder, potassium hydroxide (KOH), deionized water, and hydrochloric acid (HCl). The materials used for electrode sheets were PVDF binder, super-P conductive carbon, NMP organic solvent, and copper foil. The use of KOH followed by calcination in graphite modification aims to to induce nano- to submicron-scale porosity and expand the interlayer spacing within the graphite structure. These structural modifications enhance lithium-ion storage capacity and facilitate faster ion diffusion during charge–discharge cycles. This synthesis approach offers a simpler and lower-cost method for producing modified graphite electrodes, with strong potential to be carried out on a large scale. The process involved weighing graphite and KOH at a ratio of 1 kilogram of graphite per 100 L of KOH solvent. 85% KOH was dissolved in pure water at a concentration ranging from 0.75 to 2 M. Graphite was gradually added to the KOH solution with slow stirring. The graphite was gradually added in the KOH solution and stirred for 2 hours using an overhead stirrer at a stirring speed of 600 rpm. The resulting graphite suspension was separated from the solvent using a vacuum filter, then washed with deionized water and filtered again. The graphite was dried using a vacuum oven at 80°C for 12 hours. The graphite was calcined under a nitrogen atmosphere at 800°C for 2 hours in a tubular furnace. The modified graphite was washed with 1 M hydrochloric acid solution and deionized water repeatedly to remove any remaining potassium until the pH reached 7. The modified graphite was dried at 80°C for 12 hours using a vacuum oven. For the manufacture of modified graphite electrode sheets, a slurry consisting of graphite, PVDF binder, and conductive carbon was prepared with a formulation of 85:10:5 in an organic solvent NMP with the addition order of PVDF binder, conductive carbon, and graphite for 1-3 hours. Slurry coating was carried out using

a film coater with a coating speed of between 150-250 mm per minute with a wet thickness of between 150-250 μm. Drying of the electrode sheets was carried out at a temperature of between 100-150°C. Compaction of the electrode sheets was carried out using a calendaring tool to reduce the pores in the electrode layer so that the electrolyte wettability is better and improves electrochemical performance (Davoodabadi *et al*, 2019) at a temperature of between 40-80oC, a thickness reduction of between 5-20%, and a rolling speed of 100-250 mm per minute.

3. RESULTS AND DISCUSSION

3.1. Material Characterization Results

3.1.1. X-ray Diffraction Analysis

X-ray diffraction (XRD) analysis of graphite prior to modification reveals a characteristic layered structure typical of hexagonal graphite, consistent with JCPDS card no. 411487 (Howe *et al*, 2003). A prominent (002) diffraction peak is observed at $2\theta \approx 26.5°$, corresponding to an interlayer spacing of approximately 3.35 Å, which can be calculated using Bragg's Law ($n\lambda = 2d \sin\theta$). The sharpness and high intensity of this peak indicate a high degree of crystallinity and well-ordered layer stacking within the graphite structure. Additional, less intense diffraction peaks are detected at 42.4° (100), 44.6° (101), and 54.7° (004), further supporting the identification of a hexagonal graphite phase. The intensity ratio of the (002) peak relative to the other peaks can be employed to assess the degree of graphitization of the sample.

Following the KOH etching, sintering, and washing processes, the modified graphite exhibited significant changes while retaining its fundamental layered structure. The XRD analysis remains consistent with hexagonal graphite (JCPDS card no. 41-1487), with a noticeable shift in the (002) peak from approximately 26.5° to a lower angle, namely 26.4°. This shift indicates an increase in interlayer spacing from 3.35 Å to approximately 3.41 Å. Broadening and reduced intensity of the (002) peaks are also observed, suggesting a decrease in crystallite size or increased disorder in the stacking of graphite layers. Additionally, changes in the relative intensity of the (002) peak compared to other peaks are evident, which may be attributed to alterations in preferential crystal orientation or partial exfoliation of the graphite layers. These observations are consistent with previous reports on structural disorder and exfoliation effects in modified graphite systems. (Zhou *et al*, 2014)(Mori *et al*, 2018).

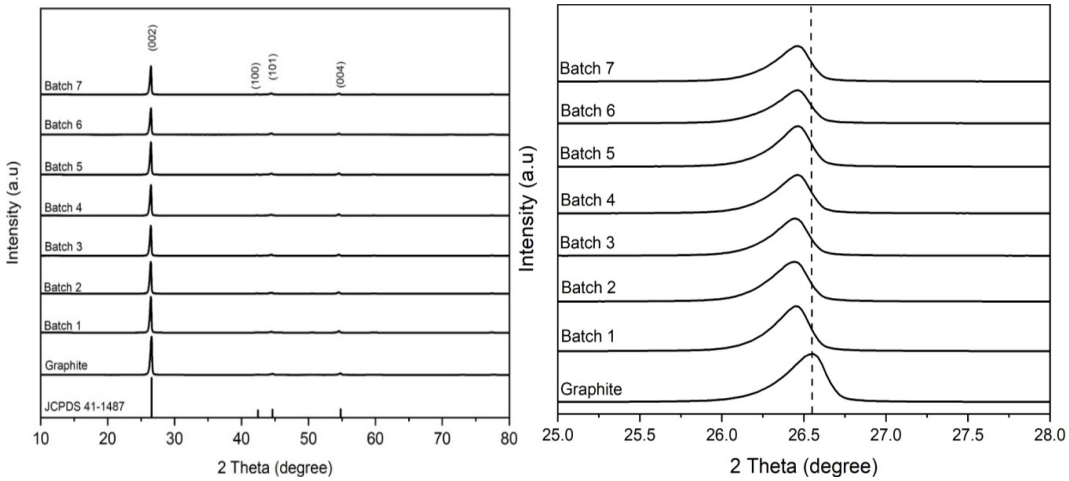

Figure 1. XRD patterns of graphite and modified graphite samples from all batches.

3.1.2. SEM/EDX Analysis

The SEM analysis of all graphite samples at 1000× magnification, as shown in Figure C, reveals bead-like particles in the micron size range, consistent with the morphology of synthetic graphite. The particles exhibit relatively smooth surfaces with minimal surface roughness. The particles exhibit a predominantly spherical morphology, with diameters ranging from 10 to 50 μm, consistent with commercial-grade graphite used in lithium-ion battery electrodes. This morphology is known to promote good powder flowability and uniform slurry dispersion, which are critical for achieving consistent electrode coating and mechanical integrity during calendaring and cycling processes (Gottschalk *et al*, 2024).

SEM images of the modified graphite at 40,000× magnification, presented in Figures C(a–g), show pronounced morphological transformations. The graphite particles exhibit more numerous and thinner lamellar layers compared to the raw graphite sample in Figure C(h), indicating successful exfoliation and surface activation, resulting in a significantly larger surface area. The sheet-like structures display irregular and jagged edges, suggesting that the KOH etching and thermal treatment effectively disrupted the basal planes and introduced edge defects. Further analysis reveals that these sheets possess lateral dimensions ranging from a few micrometers to several tens of micrometers. These features contribute to a substantial increase in accessible surface area and may enhance lithium-ion intercalation kinetics (Sumdani *et al*, 2021).

Although macropores (>50 nm in diameter) are not distinctly visible in the SEM micrographs, increased surface roughness and interlayer spacing suggest a potential increase in specific surface area. Such features are known to improve electrolyte penetration and facilitate faster ion transport, which can positively impact rate capability and capacity retention (Lv *et al*, 2014).

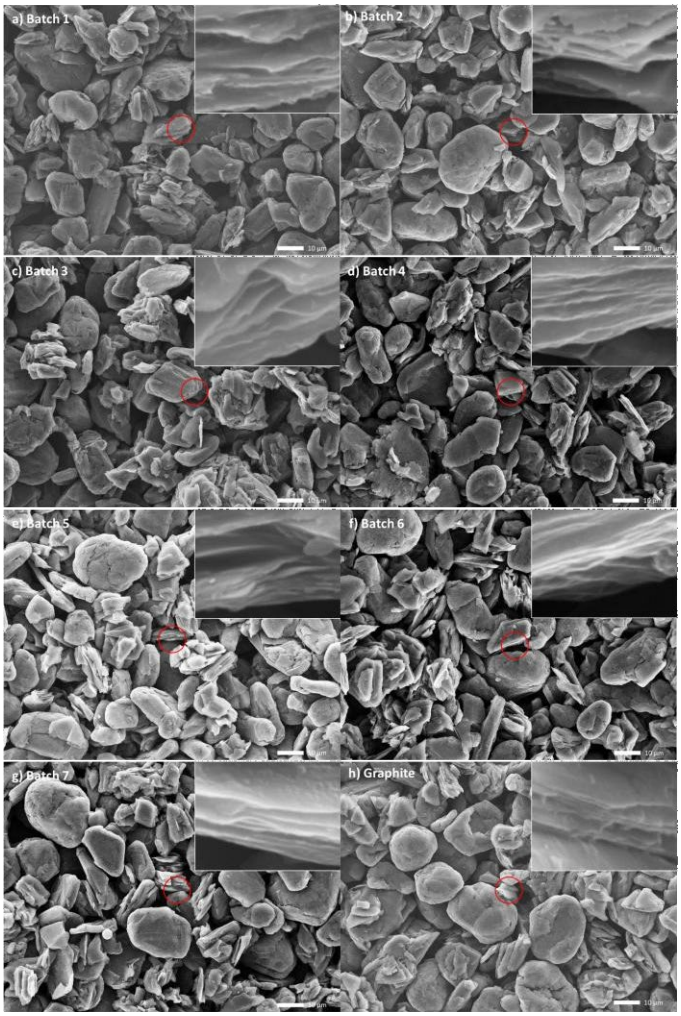

Figure 2. SEM image of the graphite sample.

Table 1. Mass percentage composition of elements in the graphite sample.

Element	**%Mass**							
	Graphite	**Batch 1**	**Batch 2**	**Batch 3**	**Batch 4**	**Batch 5**	**Batch 6**	**Batch 7**
C	98,36	98,51	98,52	99,55	97,53	97,41	99,15	99,63
O	1,64	1,49	1,48	0,45	2,47	2,59	0,85	0,37
Total	100	100	100	100	100	100	100	100

Table 1. EDX analysis results showing the elemental composition (by mass percentage) of the graphite sample. The results indicate a high graphite purity, with carbon (C) as the dominant element, comprising

97%–99% by mass. These findings are consistent with expectations, as graphite is a material composed primarily of carbon.

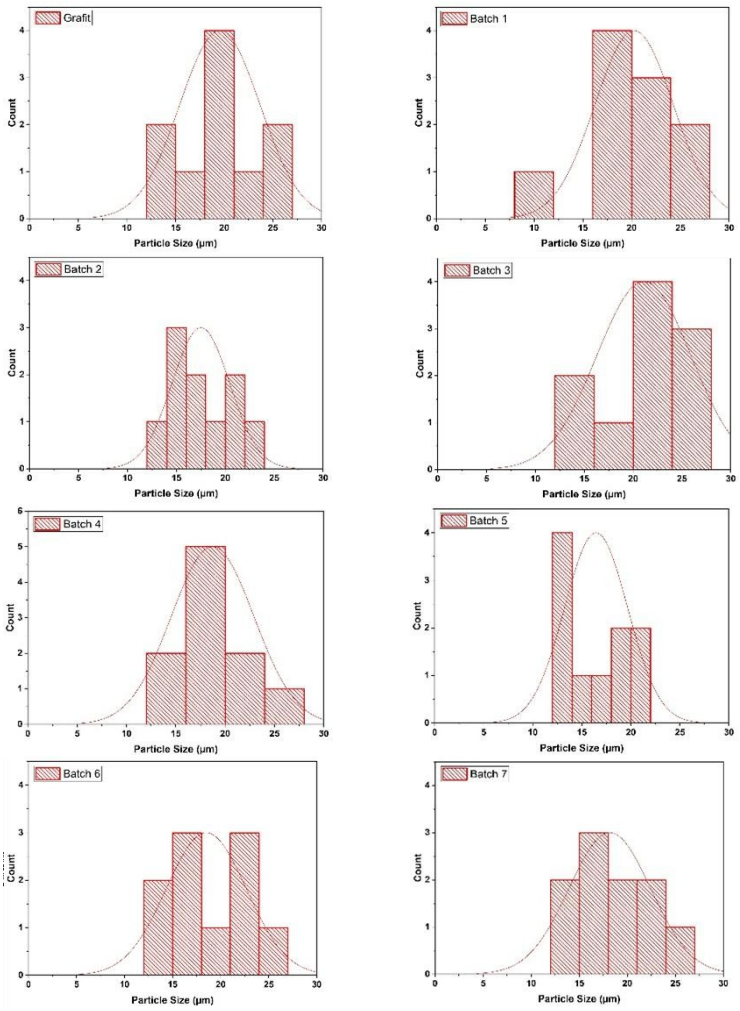

Figure 3. Particle size distribution.

3.1.3. FTIR Analysis

FTIR analysis of the graphite sample did not exhibit any distinct absorption peaks, as expected for pure graphite lacking characteristic functional groups. The obtained spectrum displays a relatively flat baseline with no significant features in the range of 4000–400 cm^{-1}. The absence of prominent peaks confirms the high purity of the graphite sample and the lack of graphite oxide or oxygen-containing functional groups on the surface. Graphite itself possesses a highly ordered and robust structure, with stable carbon– carbon bonding within its layers. This structural stability can result in weak interactions with other functional groups, potentially rendering such peaks undetectable.

The FTIR spectrum of the modified graphite similarly shows minimal absorption features, comparable to the unmodified sample. However, closer examination may reveal weak peaks around 3400 cm^{-1} (O–H stretching), 1630 cm^{-1} (O–H bending), and 1100 cm^{-1} (C–O stretching). Although these peaks are very faint, they may indicate the presence of small amounts of oxygen-containing functional groups introduced during the etching process. The very low intensity of these peaks suggests that surface modification was minimal and that the graphite structure was largely preserved.

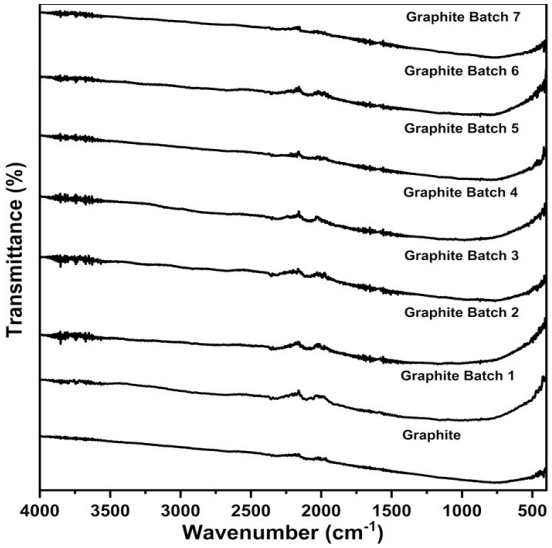

Figure 4. FTIR spectra of graphite and modified graphite samples.

3.1.4. TG/DTA Analysis

As shown in Figure 5, the Thermogravimetric and Differential Thermal Analysis (TG/DTA) conducted under a nitrogen atmosphere revealed no significant endothermic or exothermic peaks within the temperature range of 30–1000 °C. The TG curve indicates exceptional mass stability, with an average mass loss of only around 30% up to 1000 °C. This suggests very high thermal stability and the absence of volatile impurities or decomposable functional groups. The flat DTA curve further confirms the lack of phase transitions or chemical reactions during heating, which is consistent with the inert nature of pure graphite.

Similarly, TG/DTA analysis of the modified graphite prior to sintering under nitrogen atmosphere showed no prominent endothermic or exothermic peaks up to 1000 °C, indicating good thermal stability. However, a small but detectable mass loss (approximately 1–2%) was observed above 800 °C. This phenomenon may be attributed to the decomposition of residual potassium compounds potentially trapped within the graphite structure or the removal of less stable carbon atoms formed during the etching process. The DTA curve may display a very weak exothermic peak corresponding to this mass loss, indicating a minor thermal decomposition process.

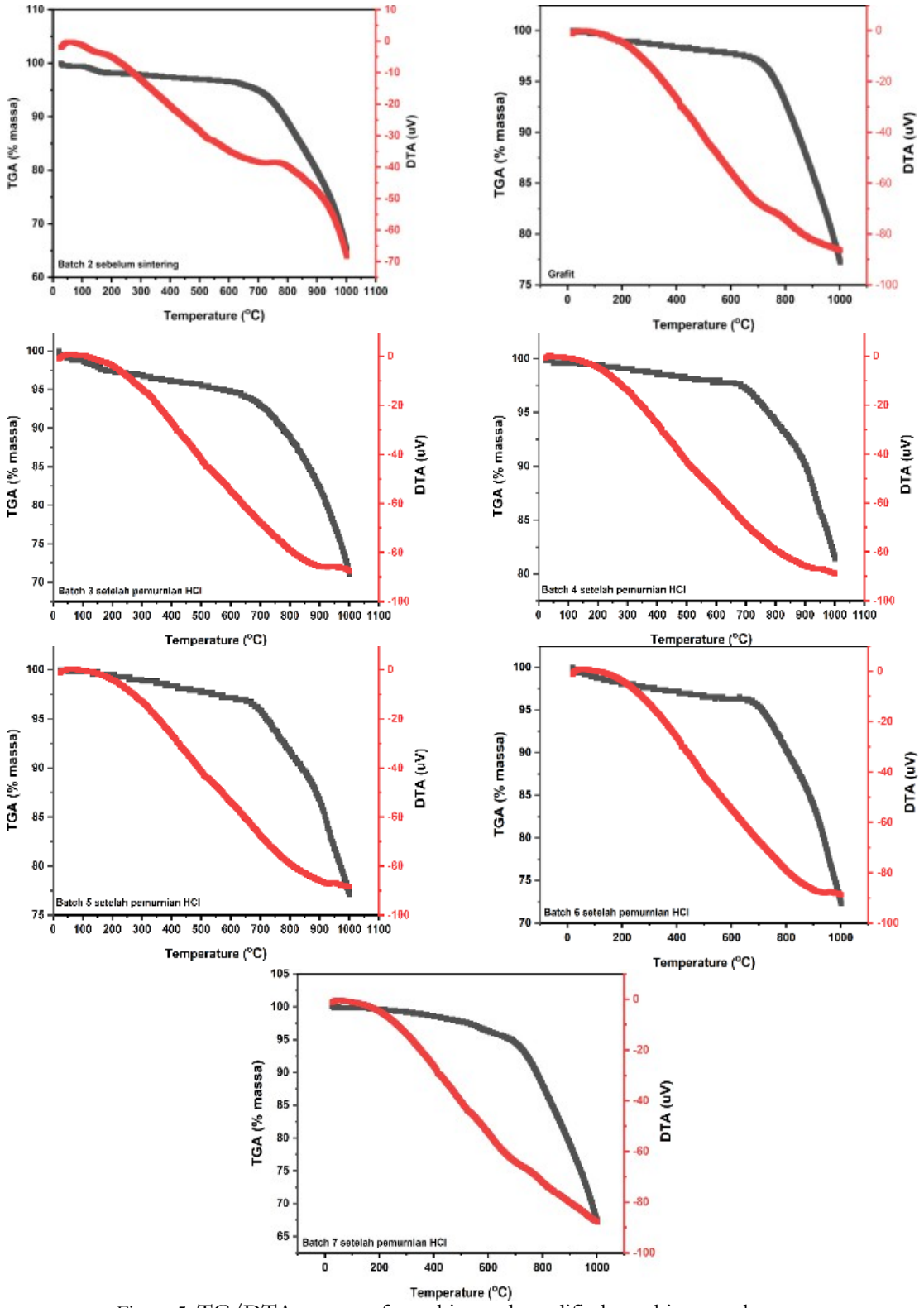

Figure 5. TG/DTA curves of graphite and modified graphite samples.

3.1.5. BET Analysis

Surface analysis using the Brunauer-Emmett-Teller (BET) method revealed a type IV nitrogen adsorption-desorption isotherm hysteresis loop, according to the classification by the International Union of Pure and Applied Chemistry (IUPAC). This phenomenon arises from the differences between the adsorption and desorption curves, which reflect the material's porous characteristics. As shown in Figure 6, several adsorption-desorption isotherm results are presented. The isotherm of graphite from batch 7

most closely aligns with IUPAC standards. The specific surface area of batch 7 graphite, as determined by BET analysis, showed a significant increase from its initial value (e.g., from 10 m^2/g to 80 m^2/g), indicating the formation of a porous structure during the modification process. The highest specific surface area was recorded at 1.816 m^2/g in the batch 5 sample.

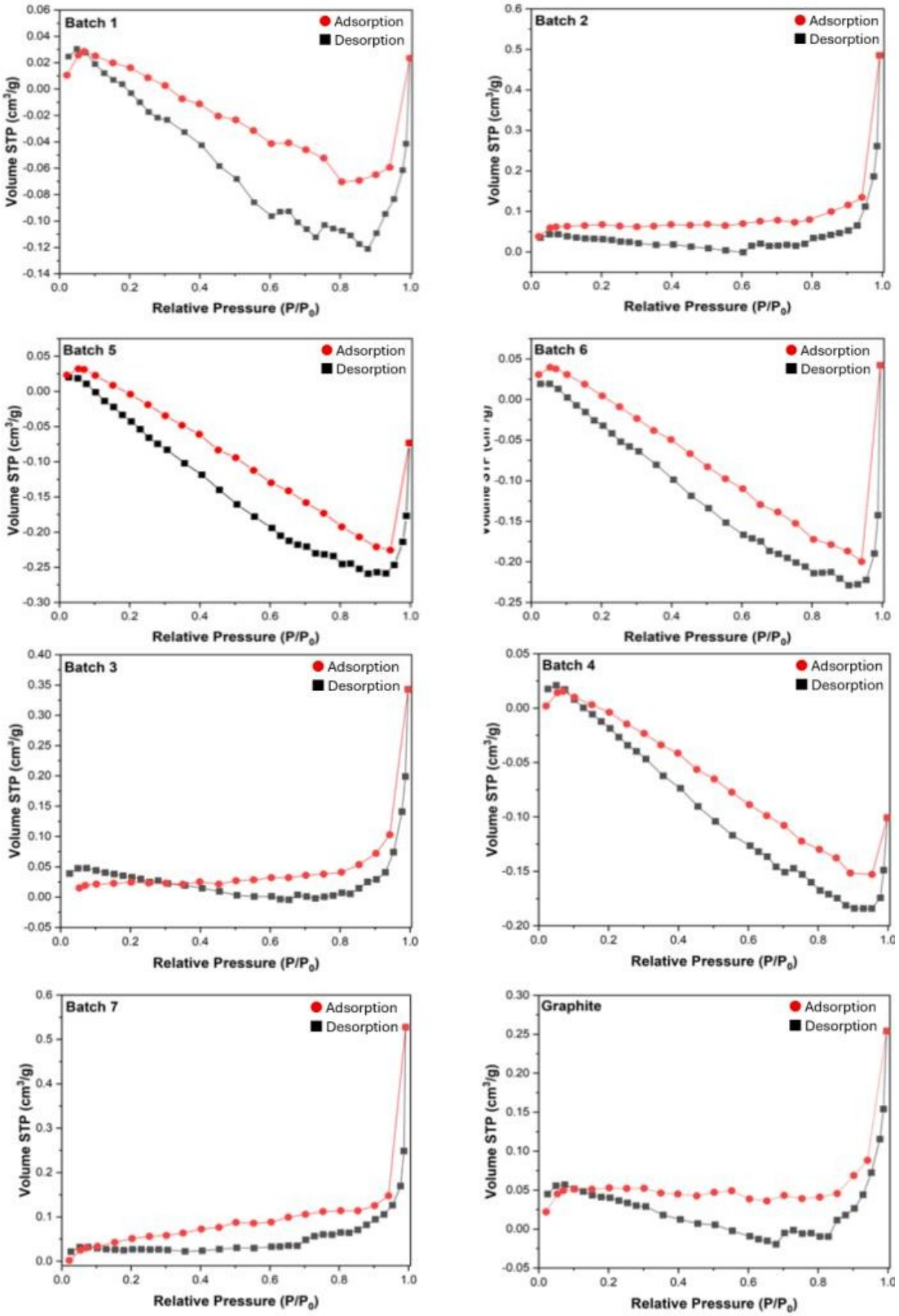

Figure 6. The results of the adsorption-desorption isotherm analysis.

3.2. Electrochemical Performance Analysis Results

3.2.1. Analysis results based on N/P

In LFP vs MG cells, there are significant variation in the N/P ratio among the six different batches, with values ranging from 1.2 to 1.8. The average N/P ratio for LFP vs MG cells is around 1.45, which is slightly higher than the generally recommended optimal ratio. From a cell performance perspective, the N/P ratio plays a crucial role in determining battery characteristics and performance. The optimal N/P ratio for LFP cells is generally in the range of 1.1 to 1.3 (Yao *et al*, 2023), with batches 4 and 5 (with ratios of 1.3 and 1.2) being closest to this ideal value. Cells with N/P ratios within this optimal range show a good balance between energy storage capacity and charge-discharge cycle stability. In addition, an optimal ratio also indicates more efficient material usage so it can optimize production costs.

Table 2. N/P Cell info LFP vs Modified Graphite (MG)

Cell	N/P
1 (batch 2)	1.44
2 (batch 3)	1.8
3 (batch 4)	1.3
4 (batch 5)	1.2
5 (batch 6)	1.6
6 (batch 7)	1.4

Batch 3, with an N/P ratio of 1.8 indicates excessive anode material usage compared to cathode capacity. Although this higher ratio can provide better cycle stability and potentially longer cell life, it is achieved at the expense of cell energy density and material utilization efficiency. It also increases the risk of lithium plating formation on the anode during charging, especially at high charge rates or low temperatures. Based on this analysis, it can be concluded that batches 4 and 5 of LFP vs MG cells are likely to show more optimal performance in terms of capacity balance and stability. From an electrochemical perspective, the higher N/P ratio of LFP vs MG cells can be explained by several fundamental mechanisms. When the N/P ratio reaches 1.8 as in batch 3, the excess anode capacity creates a significant buffer to accommodate the volume expansion during the lithium intercalation process. This buffer can mitigate mechanical stress on the anode structure, so it can extend the cell life. However, the tradeoff of that is increasing the internal impedance of the cell and in terms of economic aspects, Batch 3 (N/P 1.8) uses ~50% more anode material than batch 5 (N/P 1.2) so that the increase in production costs is not linear with the increase in performance and sustainability aspects related to the use of excess material need to be considered.

3.2.2. Lab Scale Specific Capacity Test Analysis Results

The charge-discharge curves of six Small Scale (SS) - LFP vs Modified Graphite Sintering Batch 2 to Small Scale - LFP vs Modified Graphite Sintering Batch 7 (SS - LFP vs MG SB 2 to SS - LFP vs MG SB 7) battery cells in Figure 7 reveal the electrochemical performance of LFP and modified graphite materials.

All cells operate in the voltage range of 2.5V to 3.7V which is typical for LFP-based systems, with specific discharge capacities generally reaching 140 - 150 mAh/g, indicating good utilization of the active materials. The performance variation between cells indicates that the modification process for LFP and graphite is sensitive to processing conditions. In particular, SS - LFP vs MG SB 6 shows the best overall performance, with the most symmetrical charge-discharge curves, minimal polarization, and the highest specific capacity approaching 160 mAh/g.

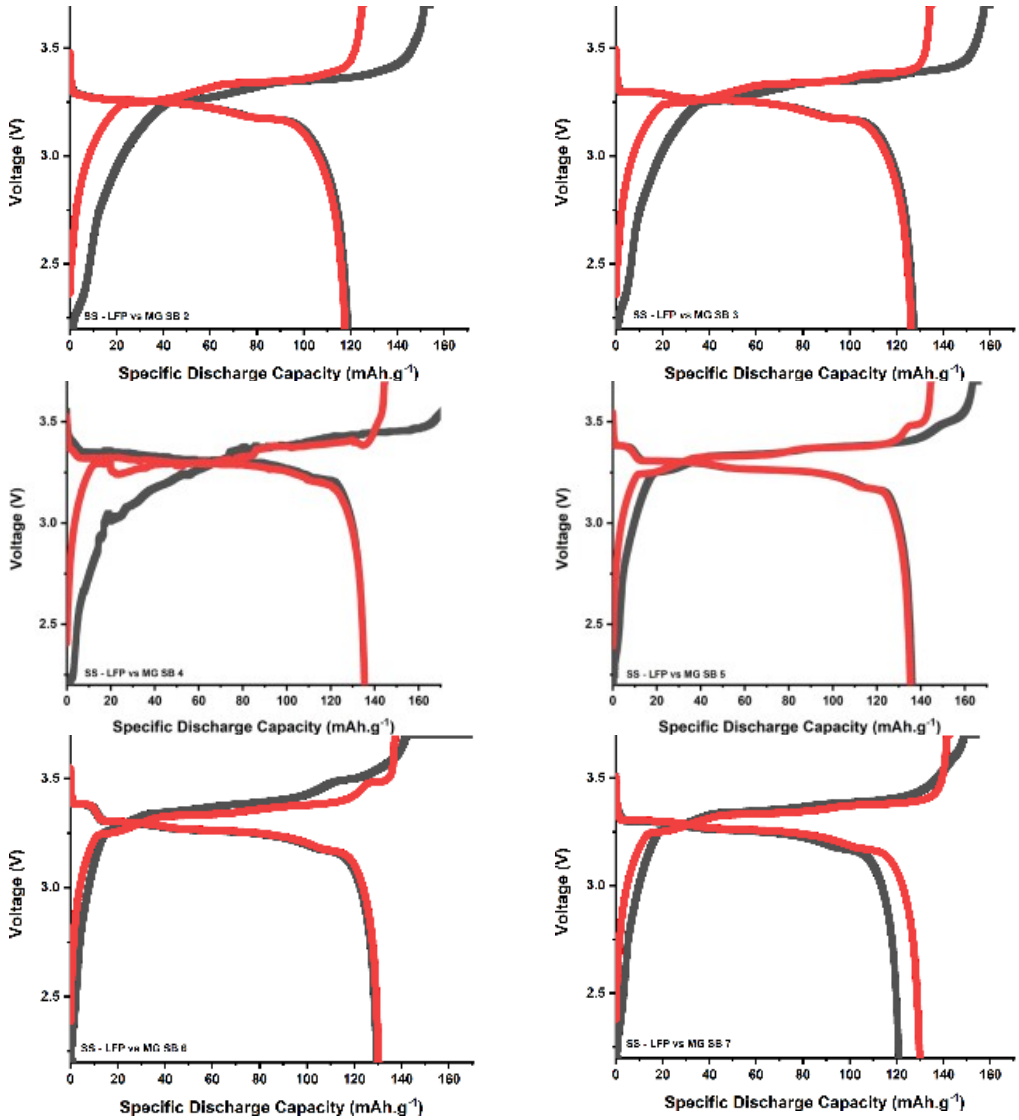

Figure 7. Lab scale capacity test results of LFP vs modified graphite of all batches.

3.2.3. Lab Scale Rate Performance Test Analysis Results

All tested battery cells showed good initial capacity, ranging between 120-140 mAh/g at 0.5C rate. Among all cells, SS - LFP vs MG SB 6 stood out with the highest initial capacity and the best capacity retention during cycling, while SS - LFP vs MG SB 2 and SS - LFP vs MG SB 4 run into faster capacity decline compared to the other cells.

In terms of rate performance, capacity decline linier with increasing C rate is a common case in batteries, and all cells showed this trend. SS - LFP vs MG SB 5 and SS - LFP vs MG SB 6 showed the best rate performance, maintaining relatively high capacity even at 5C and 8C rates. In contrast, SS - LFP vs MG SB 2 and SS - LFP vs MG SB 4 run into more significant capacity decline when tested at high rates.

The coulombic efficiency of all cells was also very high, with values above 95%, indicating good reversibility of the electrochemical reactions. SS - LFP vs MG SB 6 again demonstrated superior performance with the most consistent and highest coulombic efficiency across all test cycles and rates.

In terms of cycle stability, SS - LFP vs MG SB 5 and SS - LFP vs MG SB 3 performed very well, with minimal capacity degradation over 20 cycles, while SS - LFP vs MG SB 2 and SS- LFP vs MG SB 4 run into faster capacity degradation, especially in the final cycles. Interestingly, all cells also showed partial capacity recovery when the rate was returned to 1C after high-rate testing, indicating structural stability of the active materials.

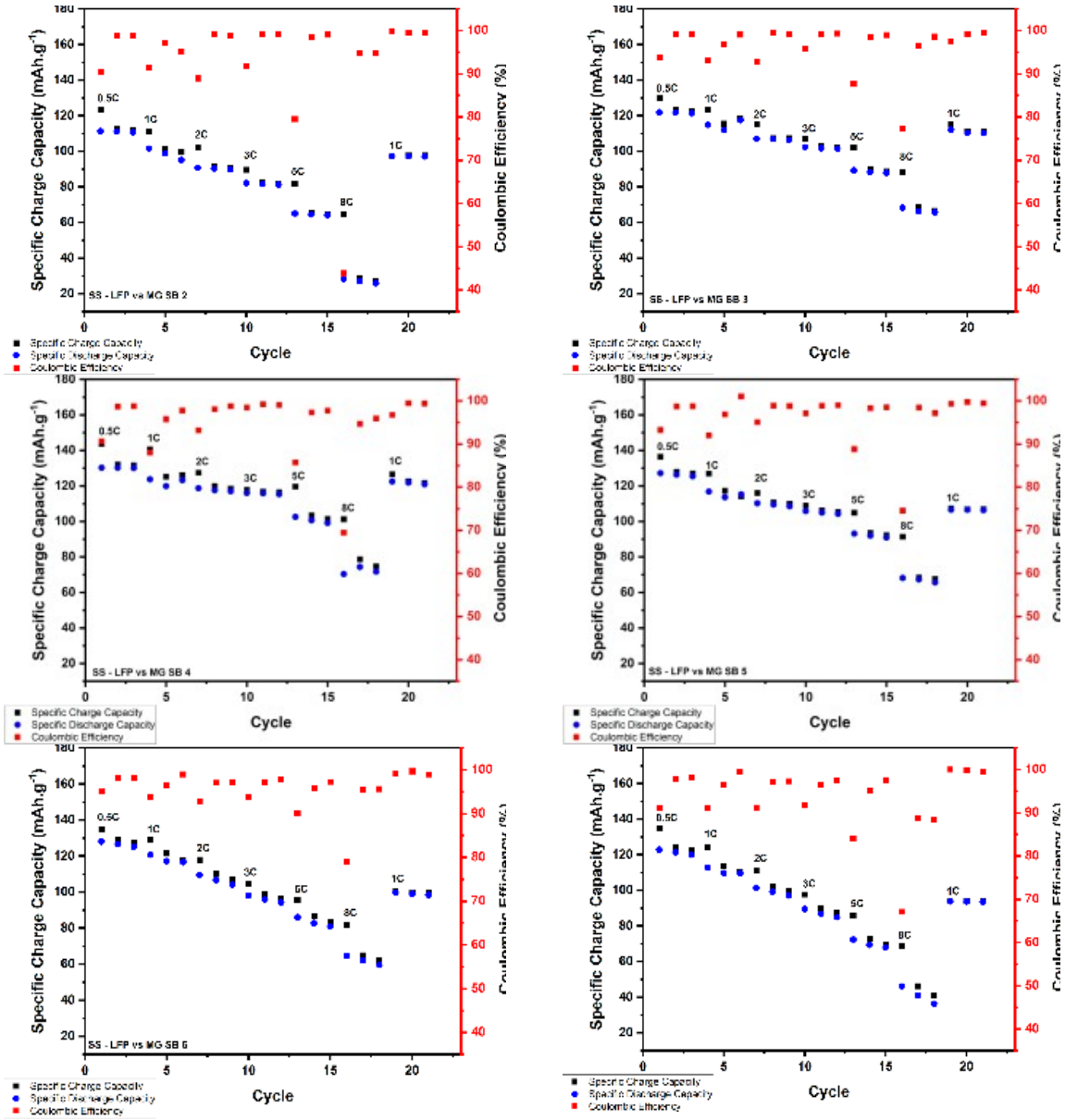

Figure 8. Lab scale capacity test results of LFP vs modified graphite of all batches.

4. CONCLUSIONS

The pilot-scale fabrication of the modified $LiFePO_4/C$ and graphite-based 18650 cylindrical cells has demonstrated enhanced energy storage capacity and stable electrochemical performance. The XRD analysis confirms the successful formation of the modified graphite anode, indicating a well-ordered graphitic structure. The Fourier transform infrared spectroscopy (FTIR) data highlights characteristic functional groups in the modified graphite materials. TG/DTA analysis reveals that the modified materials exhibit high thermal stability with minimal weight loss. SEM shows that the modified graphite anode has a porous and layered structure. This modification enhances the surface area and facilitates faster lithium-ion intercalation. The specific discharge capacity of the modified graphite and $LiFePO_4/C$ cell reaches 1.6 Ah, with high-capacity retention over 100 cycles and minimal fading. Overall, the findings from this research provide valuable insights into material optimization strategies and scalable fabrication techniques, which can contribute significantly to the advancement of next-generation energy storage systems. In the cell test, Batch 4 and 5 (LFP) showed potential sweet spots. The N/P ratio of 1-1.3 provides optimal balance.

5. ACKNOWLEDGMENT

This paper is produced based on a scale-up project of "Development of Lithium-Ion Battery Cell Prototype Based on Modified of Lithium Ferro Phosphate (LFP) Cathode Material and Graphite Anode" that has been carried out at Head Office. The project is fully supported by PT. PLN Indonesia Power.

6. REFERENCE

Amir, M., Deshmukh, R. G., Khalid, H. M., Said, Z., Raza, A., Muyeen, S. M., Nizami, A.-S., Elavarasan, R. M., & Sopian, K. (2023). Energy storage technologies: An integrated survey of developments, global economical/environmental effects, optimal scheduling model, and sustainable adaption policies. *Journal of Energy Storage*, 72, 108694.

Bao, C., Liu, Z., Yang, Z., Shi, L., He, C., Chen, H., He, Y., Liu, Q., Yang, L., & Liu, H. (2023). Constructing a boron-doped graphite anode with an accelerated Li+ diffusion dynamics for practical high-rate Li-ion batteries. *Electrochimica Acta*, 463, 142821.

Chen, R., Zhang, Y., Wang, Y., Shen, C., Zhan, L., & Ling, L. (2025). Modification mechanism of graphite anode in lithium-ion battery coated with ethylene tar pitch. *Journal of Applied Electrochemistry*, 55, 865–875.

Davoodabadi, A., Li, J., Zhou, H., Wood, D. L., Singler, T. J., & Jin, C. (2019). Effect of calendering and temperature on electrolyte wetting in lithium-ion battery electrodes. *Journal of Energy Storage*, 26. https://doi.org/10.1016/j.est.2019.101034

F. Sergi,A. Arista, G. Agnello, M. Ferraro, L. Andaloro, V.Antonucci. (2016). Characterization and comparison between lithium iron phosphate and lithium-polymers batteries J Energy Storage, 8 (2016) 235-243.

Gottschalk, L., Müller, J., Schoo, A., Baasch, E., and Kwade, A. (2024). Spherical Graphite Anodes: Influence of Particle Size Distribution and Multilayer Structuring in Lithium-Ion Battery Cells. *Batteries*, 10(2), 40.

He S, Huang S, Wang S, Mizota I, Liu X, Hou X (2021) Considering critical factors of silicon/graphite anode materials for practical high-energy lithium-ion battery applications. Energy Fuels 35(2):944–964.

Howe, J. Y., Rawn, C. J., Jones, L. E., and Ow H. (2003). Improved crystallographic data for graphite. *Powder Diffraction*, 18,150-154.

Kim, J., Nithya Jeghan, S. M., & Lee, G. (2020). Superior fast-charging capability of graphite anode via facile surface treatment for lithium-ion batteries. *Microporous and Mesoporous Materials*, 305. https://doi.org/10.1016/j.micromeso.2020.110325

Lv, L., Wu, Z., Fang, Y., Qian, X., Asiri, A. M., Tu, B., and Zhao, D. (2014). Hierarchical mesoporous/microporous carbon with graphitized frameworks for high-performance lithium-ion batteries. *APL Materials*, 2, 113302.

Mori, F., Kubouchi, M., and Arao, Y. (2018). Effect of graphite structures on the productivity and quality of few-layer graphene in liquid-phase exfoliation. *Journal of Materials Science*, 53, 12807–12815.

Ngoy, K. R., Lukong, V. T., Yoro, K. O., Makambo, J. B., Chukwuati, N. C., Ibegbulam, C., Eterigho-Ikelegbe, O., Ukoba, K., & Jen, T.-C. (2025). Lithium-ion batteries and the future of sustainable energy: A comprehensive review. *Renewable and Sustainable Energy Reviews*, 223, 115971.

Oka, H., Kadoura, H., Takahashi, N. T., & Ikawa, T. (2022). Effect of amorphous carbon coating on the formation of solid electrolyte interphase and electrochemical properties of a graphite electrode. *Journal of Power Sources*, 543, 231850.

Schultz, H., Bauer, G., Schachl, E., Hagedorn, F., & Schmittinger, P. (2000). Potassium Compounds. In Ullmann's Encyclopedia of Industrial Chemistry. *Wiley-VCH Verlag GmbH & Co.* KGaA. https://doi.org/10.1002/14356007.a22_039

Sumdani, M. G., Islam, M. R., Yahaya, A. N. A. and Safie, S. I. (2021). Recent advances of the graphite exfoliation processes and structural modification of graphene: a review. *Journal of Nanoparticle Research*, 23, 253.

Wang, Q., Mao, B., Stoliarov, S. I., & Sun, J. (2019). A review of lithium ion battery failure mechanisms and fire prevention strategies. *Progress in Energy and Combustion Science,* 73, 95–131.

Yang, M., Kim, D.-Y., & Shim, J.-H. (2024). Study on electrochemical characteristics of crystal structure changes effects of silicon anode materials for lithium ion batteries. *ECS Meeting Abstracts*, MA202401, 277.

Yao, B., Wang, Z., Ding, C., Feng, M., Li, Z., & Huang, Y. (2023). $ZnFe_2O_4$/Graphite composite with high performance as anode material for lithium-ion batteries. *Electronic Materials Letters*, 19, 29–37.

Zhou, Z., Bouwman, W. G., Schut, H., and Pappas, C. (2014). Interpretation of X-ray diffraction patterns of (nuclear) graphite. *Carbon*, 69, 17-24.